Eur. Phys. J. D **40**, 231–242 (2006)
DOI: 10.1140/epjd/e2006-00145-8

THE EUROPEAN PHYSICAL JOURNAL D

# Size dependence of freezing temperature and structure instability in simulated Lennard-Jones clusters

W. Polak[a]

Department of Applied Physics, Institute of Physics, Lublin University of Technology, ul. Nadbystrzycka 38, 20-618 Lublin, Poland

Received 12 January 2006 / Received in final form 11 May 2006
Published online 23 June 2006 – 

**Abstract.** Liquid Lennard-Jones clusters of 14 different sizes from $N = 55$ to 923 particles were cooled down to find their temperature of liquid-solid transition and the internal structure of the solidified clusters. The decrease of the cluster temperature was attained by a gradual change of the system temperature in Monte Carlo simulations. The liquid-to-solid transition was found by analysis of the specific heat as well as by detection of the structural units of face-centred cubic, hexagonal close-packed and decahedral type. It was observed that near the detected transition temperature the solid-like cluster structure is not always stable and fluctuates between solid and liquid states. The fluctuations of the state were observed frequently for small clusters with $N \leq 147$, where the temporary solid structure is created by a large part of internal atoms. Manual inspection of cluster structural data and the $10\%N$ condition for minimal number of atoms as centres of solid-like units enable detection of stable cluster solidification at freezing temperature. It was found that the freezing temperature of all clusters, with the exception of $N = 55$, decreases linearly with $N^{-1/3}$. The extrapolated freezing temperature of the bulk LJ system is 13% lower than the experimental value of argon. After freezing, the solid phase remains but some atoms close to the cluster surface are not firmly included into the structure and oscillate mainly between solid structure and disordered one.

**PACS.** 36.40.-c Atomic and molecular clusters – 64.70.Dv Solid-liquid transitions – 61.46.+w Cluster structure

## 1 Introduction

Cluster freezing is an interesting phenomenon reflecting clearly peculiar properties of limited-size system. One of the properties is a strong dependence of cluster freezing temperature $T_\mathrm{f}$ on cluster size, i.e. number $N$ of atoms or molecules. As was predicted already nearly one hundred years ago by Pawlow [1] for microcrystal melting and observed in simulations [2–4] (citation limited to melting of the Lennard-Jones clusters), the freezing temperature decreases with a decrease in cluster size. This implies that cluster freezing can be realised in two ways. One is identical to a bulk liquid-solid transition. It occurs when a hot liquid cluster is cooled down or quenched to a sufficiently low temperature. The other way is specific only for growing liquid clusters. In this case, the freezing/solidification may occur at a constant temperature $T$ when the cluster size increases, leading to a situation where the cluster temperature $T$ is lower than the actual freezing temperature $T_\mathrm{f}(N)$. Both freezing processes are connected with passing the freezing curve $T_\mathrm{f}(N)$ and can be clearly illustrated, respectively, as vertical and horizontal lines in a figure, where the freezing temperature is presented as a function of cluster size.

In order to observe cluster freezing in an experiment the clusters of $N$ atoms or molecules must be: (i) formed at a temperature higher than the actual cluster freezing temperature $T_\mathrm{f}(N)$, and (ii) cooled down or grown relatively long to cross the freezing curve. This is not an easy task to fulfil both conditions using two main experimental techniques for cluster creation. The first is cluster condensation in a supersonic flow through a nozzle into vacuum with cluster cooling achieved by adiabatic expansion of pure vapour or vapour and an inert gas. As argued by Gspann [5], the time of flight of clusters ($10^{-2}$ s) is too short to solidify metal and semiconductor clusters from pure vapour. On the other hand, the typical flight time ($10^{-3}$ s) from the nozzle to a structure-detecting electron beam is sufficiently long to solidify rare gas clusters [5]. Fortunately, the adiabatic expansion of water vapour was successfully applied to observe the freezing of water cluster at about 200 K [6]. The second technique involves a condensation cell with a stagnant or carrier gas for quenching vaporised atoms or molecules. In this case, however,

[a] e-mail: w.polak@pollub.pl

many substances, like metals with a high melting temperature, carbon or semiconducting elements, form directly solid clusters in a relatively cold gas. Measurements of the freezing temperature require melting of these clusters, which may be technically demanding. In the easier case of sodium clusters, characterised by the melting temperature close to the room temperature, it was necessary to heat them by a laser beam [7] or by thermalizing them in a buffer gas which contacts with a heated nozzle during flow [8].

Cluster formation by adiabatic expansions of a rare gas is commonly accepted [9–11] to involve creation of nanosized droplets from the cooled gas. The droplets are subsequently frozen, in a process close to the freezing by cooling, by lowering steadily the temperature of expanding gas as well as due to significant evaporation of cluster atoms. The freezing of the rare-gas cluster seems obvious, since the measured cluster temperatures of 32 K [12] and 37 K [13] are sufficiently high to maintain the smallest argon clusters (with estimated size $N \leq 55$) in the liquid state. The estimation follows from the comparison of the above experimental cluster temperatures with data on simulated melting temperatures $T_{\mathrm{m}}$ drawn by Rytkönen et al. [4] for 6 cluster sizes.

It is worth mentioning here that melting data, available more numerously in the literature than those for the freezing of clusters, can be used only for rough estimations because the melting and freezing temperature are reported to have different values [3,14]. One reason is pure technical because real simulations are not long enough to overcome possibly large energy barriers. This results in superheating of solid structures and supercooling of liquid ones leading to the hysteresis effect, where the difference between $T_{\mathrm{f}}$ and $T_{\mathrm{m}}$ can be relatively large [3]. The second reason is fundamental and is connected with cluster thermodynamics. As argued by Berry et al. [15], the coexistence of entirely solid-like and liquid-like clusters is expected in the coexistence region limited by the melting and freezing temperatures on each end with the relation: $T_{\mathrm{f}} < T_{\mathrm{m}}$.

Interpretation of experimental results or theoretical predictions is often limited by the availability of precisely determined freezing curve. To the author's knowledge, there is a lack of experimental data for free rare-gas clusters, while for others clusters the data are sparse [6]. Theoretical predictions are limited to give a general formula with a number of unknown constants. An overview of theoretical results was given recently by Baletto and Ferrando [11]. Therefore, the unique efficient methods are often computer simulations of freezing. Depending on cluster type, they may involve more or less complicated simulations using ab initio methods or many-body potentials, for example, for some metal clusters [16–20] as well as a pair potential modeling of interatomic/intermolecular interactions in the case of ionic-salt [21,22], molecular [23] and the rare-gas clusters [10,24,25]. Surprisingly, in spite of the simplicity of interatomic interactions represented typically by the Lennard-Jones potential or sometimes by the Morse potential, the freezing temperature data for rare gases are rarely presented for any cluster size [14,24,25]. Moreover, until now no formula with precisely given parameters enabling calculation of $T_{\mathrm{f}}(N)$ has been reported. This is in contrast to computationally more complicated systems like melting of Pb clusters [26].

The purpose of this article is precise determination of the freezing temperature for more numerous cluster sizes in the range $55 \leq N \leq 923$. This cluster size range is very promising for the observation of the size-dependence of cluster structure in view of the reported structural transition at $N \approx 450$ [10]. For the sake of precision, the freezing temperature is obtained from 21 independent simulation runs for each of the 14 analysed cluster sizes. Therefore, the total number of the obtained and the analysed clusters is near 300. The relatively close cluster-to-cluster separation, as expressed by difference in the number of cluster atoms, enables better precision in the determination of size effects on cluster structure and freezing temperature than any of the existing works in the literature. Moreover, a quite new and sensitive method is applied to detect the onset of liquid-solid transition. This uses a cluster structural analysis based on the coordination polyhedron method [27], which is able to detect the creation of first structural units typical for solid-like clusters. To compare the results, the transition temperature is obtained independently by analysing a peak position in the specific heat of a cluster. The structural analysis will be applied to observe frequent events of complete instability of newly-formed solid structure in cooled clusters above the freezing temperature. The-back-and-forth fluctuations of the cluster state between liquid and solid have their implications on terms used in this work. Here, the freezing is understood as a definitive liquid-solid transition when a formed solid cluster does not transform again to liquid one.

The paper is organised as follows. A description of the simulation method of cluster cooling is given in Section 2. Presentation and discussion of the obtained results is contained in Sections 3, 4 and 5. For a clarity of presentation, the transition temperatures of all clusters are obtained first in Section 3 by analysing the specific heat peak, and then in Section 5 by applying the structural analysis. Section 4 is devoted to an exhaustive discussion of the problem of structural instability which is necessary to understand difficulties in determining the cluster freezing temperature. Finally, Section 6 summaries the main findings of the work.

## 2 Simulation method and analysis procedures

The general concept of cluster cooling simulations is based on our previous work [27] in which the cluster formation, equilibration and heating were discussed. Cluster cooling is realized here by a gradual decrease in the system temperature $T$, while the remaining two system parameters, volume $V$ and number of particles $N_{\mathrm{sys}}$, are kept constant. This means that, at a given simulation stage when $T$ is constant, the canonical Monte Carlo method can be used.

Particles (also called atoms below) interact via the Lennard-Jones 6-12 potential:

$$U_{\mathrm{LJ}}(r) = 4\varepsilon \left[ \left(\frac{\sigma}{r}\right)^{12} - \left(\frac{\sigma}{r}\right)^{6} \right], \qquad (1)$$

where $r$ is the interparticle distance, while $\sigma$ and $\varepsilon$ are potential parameters, the values of which for different rare-gas atoms can be found easily in the literature [28]. In the reported simulations, the potential is truncated at distance $r_{\mathrm{tr}} = 3.4\sigma$ without shift. The LJ potential parameters are used also to express results in dimensionless reduced units: reduced distance $r^* = r/\sigma$, reduced energy of the system $U^* = U/\varepsilon$ and reduced temperature $T^* = k_{\mathrm{B}}T/\varepsilon$ with $k_{\mathrm{B}}$ as the Boltzmann constant. Using the value of $\varepsilon = 1.67\times10^{-21}$ J [28], one obtain the relation between absolute and reduced temperature for argon as: $T = 121 \times T^*$ [K].

A simulation cell of edge length $L$ was repeated periodically in the 3-dimensional space to enable periodic boundary conditions, where atoms can freely pass the simulation cell border and interact not only with atoms in the cell but also with images of atoms. Random movements of atoms, present in MC simulations, are governed by the Metropolis criterion giving acceptance probability $p$ of an atom displacement:

$$p = \exp\left(-\Delta U/k_{\mathrm{B}}T\right), \qquad (2)$$

where $\Delta U > 0$ denotes the change (here an increase) in the interactions energy due to the analysed atom displacement. In case when $\Delta U < 0$, always $p = 1$. In every MC cycle, there were $N_{\mathrm{sys}}$ attempts to displace an atom, each time randomly selected from $N_{\mathrm{sys}}$ atoms in the system. The maximum allowed atom displacement in one direction $\Delta x$ is adjusted here to obtain the acceptance probability $p$ close to 0.4 when averaged for the system in one MC cycle.

In contrast to our previous work [27], cluster translation or rotation was not included in simulation algorithm. Therefore, cluster position described by its centre of mass can change (see insets in Fig. 1) only due to displacement of single atoms. The initial cluster of a given size was obtained by random location of $N_{\mathrm{sys}}$ LJ atoms in a cubic central part of simulation cell (stage A in Fig. 1), as used previously [27]. After thermal equilibration at sufficiently high temperature $T_l^*$ during many MC cycles (typically 600 000 to 1 000 000 for large clusters), the liquid cluster is obtained (stage B). During simulations, at every moment atoms can evaporate from the cluster into surrounding space when it is accepted by the Metropolis criterion. Similarly, the vapour atoms can join/adsorb the cluster, if they approach the cluster at a distance less than $R_{\mathrm{cl}}^* = 1.5$ during their random walk.

In order to achieve cluster cooling, MC simulations were realised along the path of gradually decreasing temperature (B-C-D in Fig. 1). The cluster cooling-down process was realised by: (a) selecting a final cluster with all vapour atoms (if they exist) obtained at a given high temperature $T^*$, (b) thermalising such a system at the decreased temperature $T^* - \Delta T^*$ during at least 100 000 MC cycles, and (c) calculation of all quantities of interest, averaged over the subsequent 100 000 or 200 000 MC cycles. The cooling process was terminated always at $T^* = 0.05$ (stage D), where structural changes in the cluster cease.

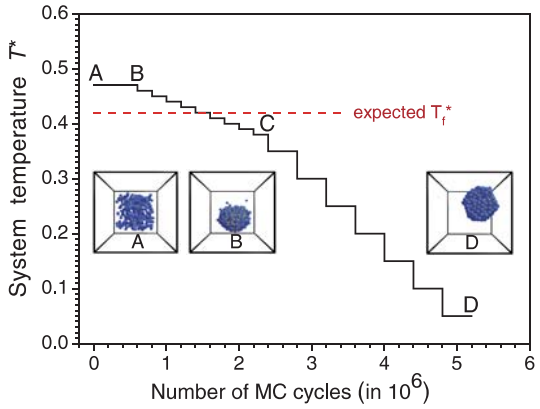


**Fig. 1.** (Colour online) Plot of changes in the system temperature $T^*$ during the simulated cluster cooling. Main stages of the cooling are: (A) initial cluster composed of $N$ (here $N = 450$) randomly-located atoms in the centre of simulation cell, (B) a liquid cluster obtained after thermal equilibration of the initial cluster at a sufficiently high temperature, (B-C-D) the region of gradual change in the system temperature in the temperature range around expected phase transition (B-C) and after the freezing (C-D), (D) the solid cluster at the final temperature of $T^* = 0.05$.

LJ clusters of 14 different sizes from $N = 55$ to 923 were cooled down. The number of atoms was chosen to be equal to the size of: (a) the Mackay clusters ($N = 55$, 147, 309, 561 and 923), (b) the fcc truncated octahedron with $N = 201$, (c) the Marks decahedron with $N = 75$, and (d) $N = 62$, 81, 110, 222, 450, 700 and 810 not related with any magic number. To obtain a precise value of the cluster parameters (e.g. freezing temperature) in the expected transition region, the system temperature was changed after each 200 000 MC cycles by $\Delta T^* = 0.01$ as shown in Figure 1. Apart from this region, 400 000 MC cycles and $\Delta T^* = 0.05$ were applied. These simulations were carried out 21 times, each time starting from the same liquid cluster (cluster B from Fig. 1) of analysed size $N$ but with a different seed in the random number generator. The initial liquid cluster was proved by structural analysis to exclude precritical nuclei of solid phase.

In each temperature stage during cluster thermal equilibration, parameters of the system like the binding energy per atom $U^*/N_{\mathrm{sys}}$, the specific heat, the radial distribution function and the cluster distribution were calculated. Moreover, for the most frequently found cluster size $N$, averaged values of the number of centres $N_{\mathrm{str}}$ of local atom ordering in the cluster were calculated and stored together with the number of internal atoms characterised by a presence of minimum 12 neighbours up to $R_{12\mathrm{n}}^* = 1.55$. The lower index 'str' means fcc, hcp, ic, dh or bcc, which signify: face-centred cubic (fcc), hexagonal close-packed (hcp), icosahedral (ic), decahedral (dh) and bulk-centred cubic (bcc) structures.

An atom was assumed to be the centre of local structure if its neighbouring atoms from the first coordination shell form a regular coordination polyhedron [27] typical for fcc, hcp, ic, dh and bcc structures. Deformations of the coordination polyhedron shape are accepted if it does not lead to formation of a new edge between excessively approached atoms. When it occurs, the central atom is classified to have an irregular local structure. Since bcc centres were found very rarely in comparison with other structures, their analysis was excluded from this work. However, the presence of a bcc unit in a cluster snapshot is seen, without author's intention, in one of the figures below. The structural units in the case of fcc, hcp, ic and dh local structure means a group of 13 atoms, i.e. a central atom and 12 its closest neighbours in the first coordination shell. The structural units existing in a cluster were detected using the coordination polyhedron method [27], where a sphere radius in the range $1.15 \leq R_{\mathrm{n}}^{*} \leq 1.55$ and a radius increment $\Delta R_{\mathrm{n}}^{*} = 0.10$ were applied for detection of atoms with a regular coordination polyhedron shape. Two structural units may be separated from each other, contacted (some neighbours are common) or interpenetrated (the central atom of one local unit belongs to the second unit). As in the previous work [27], cluster atom ordering is visualised by presenting the central atoms of all units.

## 3 Determination of transition temperature from specific heat peaks

There are many reports in the literature (e.g. see Refs. [21,25,27,29]) where phase transitions in clusters were successfully investigated using specific heat curves. According to these reports, cluster phase change occurs at a temperature corresponding to the maximum of the specific heat $C_{\mathrm{V}}$. Therefore, it was decided here to monitor each simulation run of the reported cluster cooling by saving the specific heat (in the reduced unit $k_{\mathrm{B}}$/atom) of the system. It was calculated from the relation

$$C_{\mathrm{V}} = \frac{3}{2} + \frac{\langle (U^{*})^{2} \rangle - \langle U^{*} \rangle^{2}}{N_{\mathrm{sys}} (T^{*})^{2}}, \qquad (3)$$

where the first term 3/2 denotes impact of the kinetic energy not present in MC computations, while the second term originates from the system potential energy and is calculated here from fluctuations in $U$ (the angular brackets denote averaging of the corresponding value). Identical to other parameters of the analysed system or cluster, the averaging of $U^{*}$ and $(U^{*})^{2}$ started after the thermal equilibration period. As mentioned before, the length of each period equals 100 000 or 200 000 simulation cycles, depending on the cooling stage.

In the case of specific heat calculations of unstable system (when the phase transition occurs), unfortunately, the calculations were able to detect precisely the transition only if it occurred during the averaging period. From the analysis of the obtained specific heat curves it became evident that only a part of them shows a pronounced maximum attributed to the cluster structural transition from liquid to solid state, while the remaining curves are characterised by a certain number of low-lying local maxima. Two typical examples of different curves are compared in Figure 2a to illustrate the difficulty in the determination of the transition temperature when several peaks are present.

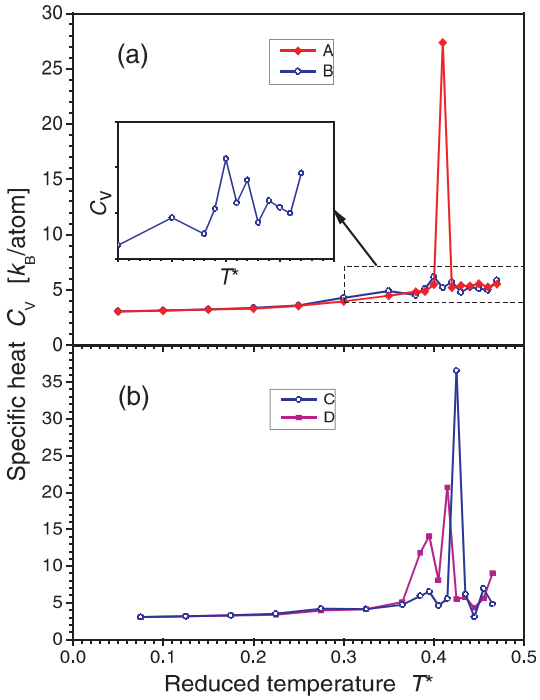


**Fig. 2.** (Colour online) Two types of the specific heat curves characterised by: (A, C) one dominating maximum, and (B, D) two or more low-lying local maxima (maxima of B are shown more distinctly in the inset). $C_{\mathrm{V}}$ values were calculated for the cluster size $N = 450$ using (a) equation (3), and (b) equation (4). Curves B and C represent the same cluster cooling simulation while A and D refer to two different clusters.

The question now is: which peak should be chosen to be related with the cluster solidification? Each decision could be regarded as arbitrary. Fortunately, the determination of the cluster liquid-solid transition using the specific heat curves were planned to be only auxiliary, while the structural analysis of cluster structure was decided to be fundamental. The latter method (presented in detail in Sect. 5) proved to be sensitive even if cluster liquid-solid changes occur during the thermal equilibration. Therefore, the analysis of cluster phase transition was based mainly on the structural analysis, while the unquestionable global maxima on the specific heat curves carried some additional data for comparison. Moreover, using both methods more effort was made in Section 4 to understand reasons for the creation of smaller peaks.

After limiting interest to the specific heat curves characterised by one dominating maximum, it was possible to determine the transition temperature $T_{\mathrm{tr}}^{*}$ (see Tab. 1) in prevailing number $N_{\mathrm{select}}$ in the range from 8 to 17 (dependent on cluster size) of 21 simulation runs selected for every cluster size $N$. As in the case of cluster melting

**Table 1.** Averaged liquid-solid transition temperature $\langle T^*_{\rm tr}\rangle$ of LJ clusters as obtained from analysis of the maximum position in specific heat $C_{\rm V}$ calculated according to relation from (a) equation (3), and (b) equation (4). Other parameters are explained in the text.

| $\langle N(T^*_{\rm tr})\rangle$ | (a) | | (b) | | $\langle N_{\rm V}(T^*_{\rm tr})\rangle$ |
|---|---|---|---|---|---|
| $N_{\rm sys}$ | $\langle T^*_{\rm tr}\rangle$ | $\Delta T^*_{\rm tr}$ | $\langle T^*_{\rm tr}\rangle$ | $\Delta T^*_{\rm tr}$ | |
| 55 | 0.297 | 0.017 | 0.292 | 0.023 | 0.00 |
| 62 | 0.289 | 0.022 | 0.272 | 0.023 | 0.00 |
| 75 | 0.303 | 0.023 | 0.292 | 0.013 | 0.01 |
| 81 | 0.300 | 0.030 | 0.301 | 0.016 | 0.00 |
| 110 | 0.327 | 0.017 | 0.321 | 0.016 | 0.00 |
| 147 | 0.348 | 0.018 | 0.341 | 0.026 | 0.05 |
| 201 | 0.370 | 0.020 | 0.374 | 0.011 | 0.12 |
| 222 | 0.383 | 0.013 | 0.382 | 0.023 | 0.07 |
| 309 | 0.404 | 0.024 | 0.404 | 0.029 | 0.05 |
| 450 | 0.420 | 0.030 | 0.425 | 0.020 | 0.16 |
| 561 | 0.433 | 0.017 | 0.436 | 0.021 | 0.31 |
| 700 | 0.451 | 0.021 | 0.452 | 0.023 | 0.44 |
| 810 | 0.448 | 0.018 | 0.449 | 0.016 | 0.34 |
| 923 | 0.452 | 0.018 | 0.453 | 0.018 | 0.31 |

analysed by theoretical predictions [11] and reported simulation data [4], the value of $T^*_{\rm tr}$ is strongly size-dependent and shows a significant decrease with a decrease in the number of cluster atoms $N$. All transition temperature data are accompanied by uncertainty errors $\Delta T^*_{\rm tr}$ estimated here as the distance between the averaged and most separated value of $T^*_{\rm tr}(N)$.

As mentioned above, the specific heat $C_{\rm V}$ calculated from fluctuations in the system energy according to equation (3) often reveals only small maxima which are useless when only one transition temperature is searched. Therefore, the other alternative for calculating $C_{\rm V}$ directly from the averaged potential energy $\langle U^*\rangle$ (stored at every temperature stage) was realised using the simple equation

$$C_{\rm V}(T-\Delta T/2)=\frac{3}{2}+\frac{\langle U^*(T-\Delta T)\rangle-\langle U^*(T)\rangle}{N\Delta T}. \quad (4)$$

The $C_{\rm V}$ data obtained in this way lead to curves with usually one dominating maximum as illustrated by the curve C in Figure 2b. This is a general picture in the case of larger clusters with $N \geq 561$. However, for $N \leq 450$ some $C_{\rm V}(T^*)$ plots also reveal several smaller local maxima as shown by the curve D in Figure 2b. Every maximum corresponds to a temperature where the potential energy change during cooling is significantly large. When the dominating maximum is interpreted to be caused by the solidification, the transition temperature $T^*_{\rm tr}$ can always be easily determined.

When one compares the values of the transition temperature from Table 1 obtained using equations (3) and (4) for a given $N$, a good agreement between the two data is observed, because the difference in $T^*_{\rm tr}$ is significantly lower than the uncertainty errors $\Delta T^*_{\rm tr}$. However, it must be remembered that from statistical point of view the analysis of $C_{\rm V}(T^*)$ curves obtained from equation (4) gives more precise results since averaging of $T^*_{\rm tr}$ for a given $N$ was done over all 21 simulation runs instead of near half in the case of equation (3).

The other data from Table 1, the mean number of vapour atoms $\langle N_{\rm v}(T^*_{\rm tr})\rangle$ in the cell of the edge length $L^* = 20.4$, is given to discuss the impact of atom vaporisation on the average cluster size $\langle N(T^*_{\rm tr})\rangle$ near the transition temperature. The cluster size is not identical with the precisely determined and constant number $N_{\rm sys}$ of atoms in the system due to atom evaporation from a cluster. However, it may be seen that the cluster evaporation is relatively low and practically does not change the cluster size at solidification since $N_{\rm v} < 1 \ll N$ for the cluster sizes analysed here. Such small intensity of evaporation does not influence the value of the system specific heat.

## 4 Instability of cluster structure near the state transition temperature

Important insight into changes in the cluster structure was gained by two methods. The first method is based on an analysis of the number of the structural units present in a cluster using data stored every 2000th MC cycle. The analysis is done at selected simulation stages connected with significant peaks in the specific heat. The second method is based on the examination of images of an arrangement of the structural units in the cluster at selected interesting simulation cycles. Cluster states are easily detectable, because in liquid clusters the structural units are usually sparse and separated, while in solids they are much more numerous and interpenetrated. Moreover, changes in the structure of solidified clusters can be precisely observed. However, for the visualisation of an interesting arrangement of cluster atoms, repetition of simulations was necessary to write positions of atoms at a chosen simulation stage.

Not only global maximum, but all significant peaks were targeted for the detailed structural analysis. The comparison revealed that the first peak is often a result of a temporary solid structure formation. This is illustrated in Figure 3 for three different cluster sizes: 55, 201 and 700 atoms. One can see that a solid-like structure (the central snapshot for each cluster) is formed from the liquid-like cluster (on left) and disappears (on right) after a short, in comparison with the averaging period, simulation time.

It should be noted that none or only icosahedral local units are present in two smaller clusters (Figs. 3a and 3b) in the beginning of the averaging period. The same situation exists at the end when solid structure disappears. The larger clusters may sometimes show initially single solid-like structural units apart from several icosahedral units which are practically always present. This is shown in Figure 3c for the cluster with $N = 700$, where one can observe in the beginning of the averaging period at 100 000 MC cycle the structure containing 1 hcp, 1 dh and 9 ic units. Then, at a certain moment of simulations, a solid-like cluster structure is formed, where fcc and hcp

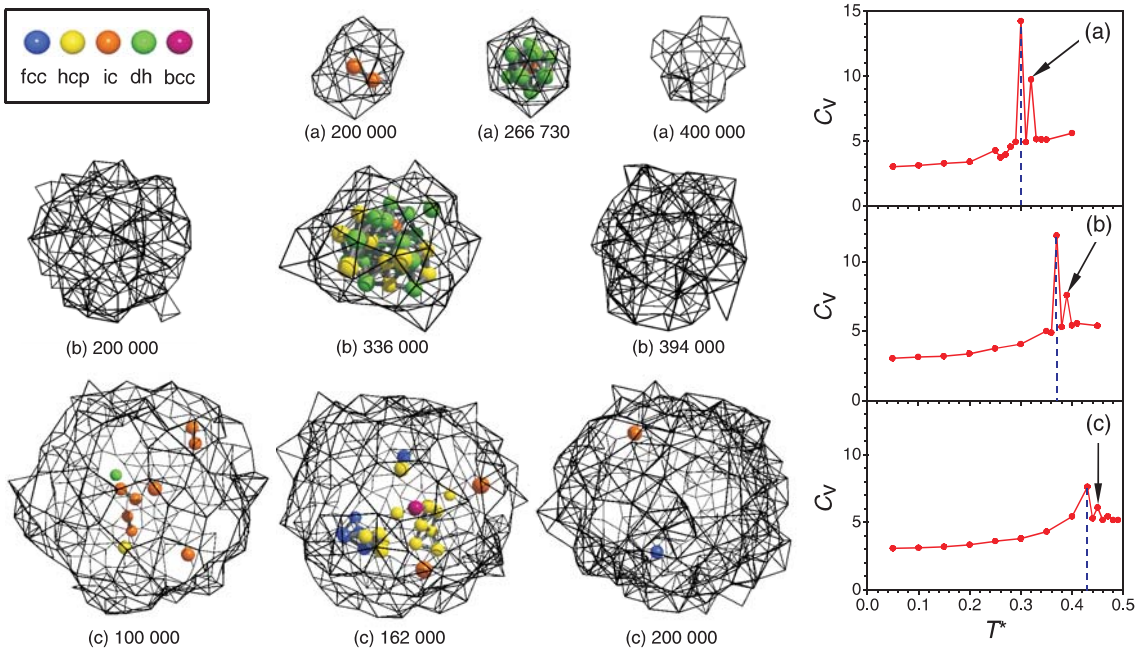


**Fig. 3.** (Colour online) Examples of complete instability of solid-like phase (the central snapshot for each cluster) observed in clusters with: (a) 55, (b) 201, and (c) 700 atoms. Snapshots of cluster structure are taken at simulation time measured and shown in number of MC cycles from the beginning of thermal equilibration at an analysed temperature. Temperature for each cluster is pointed by arrow in the specific heat curve, while the detected freezing temperature is shown by dashed line.

units are the building blocks of this solid phase. Finally, at 200 000 MC cycle only one fcc and one icosahedral unit were registered.

The unstable solid structure may be created by: (i) a dominant number of the cluster internal atoms (small clusters with $N \leq 147$), (ii) large part of the internal atoms in case of medium-sized clusters with $N = 201$, 222 and 309, or (iii) only a small part of the internal atoms for $N \geq 450$. After a certain simulation time, the solid structure completely disappears in the case of smaller clusters or appears from time to time only as single solid-like structural units. For cluster sizes $N \leq 309$, the structural transitions between solid-like and liquid-like cluster state and vice versa can be understood as manifestation of metastability of the cluster structure in its pure liquid or solid form before the cluster freezing. Such structural transitions are called as the fluctuations of state. The observed structural instability of larger clusters is connected here with partial instability of liquid cluster by the creation of unstable small solid domains inside stable liquid medium (see Fig. 3c at 162 000 MC cycle). The temperature of the shown clusters is always higher than $T^*_{\rm tr}$ as can be read off from the temperature scale on the plots of the specific heat in Figure 3. However, detailed structural analysis (explained in next section) is needed to prove if the resulting solid-like structure below $T^*_{\rm tr}$ does not disappear and we really observe freezing at $T^*_{\rm f} = T^*_{\rm tr}$ instead of temporary solidification.

The metastability of cluster state is explained as a result of natural coexistence of solid-like and liquid-like clusters in the temperature range between $T_{\rm f}$ and $T_{\rm m}$ as predicted first by Berry et al. [15,30,31] from estimations of the cluster Helmholtz free energy. The predictions were confirmed by Honeycutt and Andersen [24], Sugano [29] and Matsuoka et al. [32] in simulations of small LJ clusters with $N \leq 147$. More instructive for the interpretation of the results in the case of larger clusters are results given by Nam et al. [19]. They observed the formation and dissolution of very small embryos with hcp, fcc and five-fold local symmetries in a liquid 561-atom gold nanocluster. This structural behaviour of the gold cluster is similar to that of larger LJ clusters, illustrated in this paper for 700 atoms in Figure 3c. Here the fcc, hcp, ic or dh local structures were registered in the form of isolated structural units or units joined together to a nucleus as shown in the central snapshot in Figure 3c. They are not stable and disappear (generally with the exception of icosahedral unit) in the course of simulations.

Differences in structure instability inside large and small LJ clusters, reported here, may be understood by using the concept of 3 types of phase coexistence: static, transient and dynamical, as used recently by Schebarchov and Hendy [33] for explaining phase coexistence in simulated metal (Ag, Cu and Ni) nanoclusters. In this context, the creation and disappearance of a relatively low number of the solid-type structural units in the larger LJ clusters ($N \geq 450$) analysed here can be understood as a manifestation of the transient coexistence between solid-liquid and stable liquid state. However, structural changes in the small LJ clusters can be explained as the dynamical coexistence since a liquid-like or solid-like structure created temporarily can reach the size of the entire cluster.

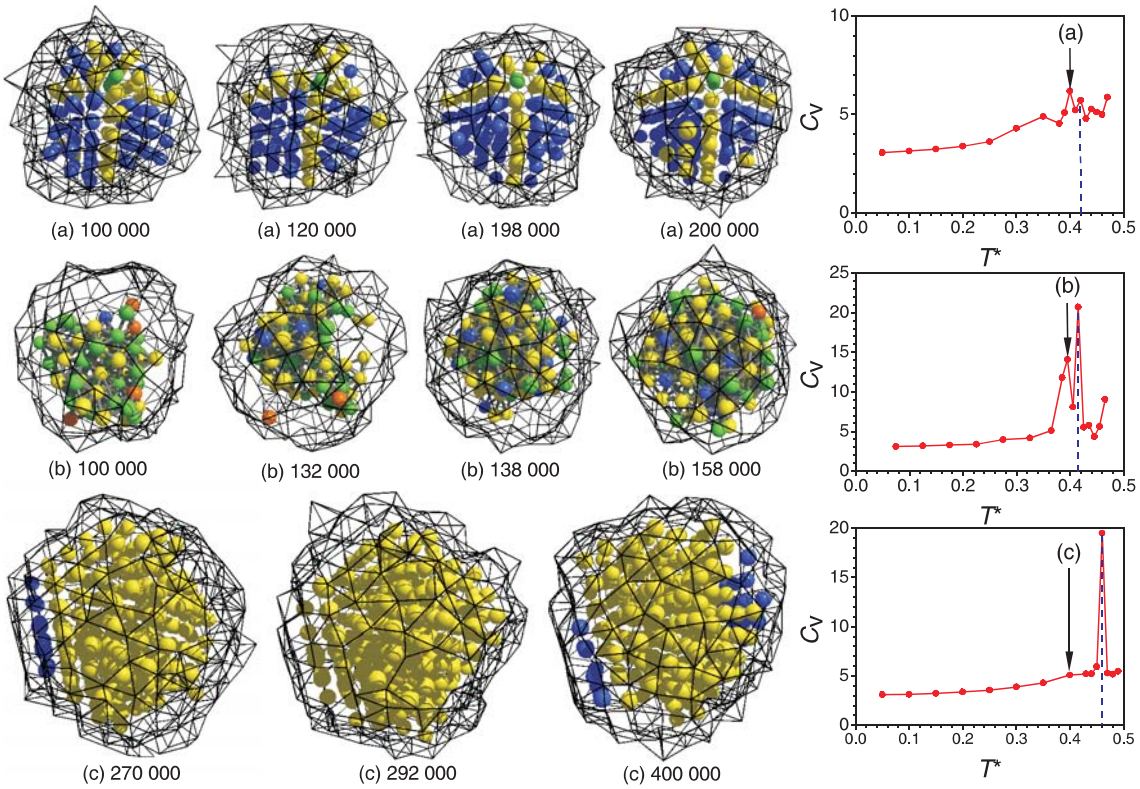


**Fig. 4.** (Colour online) Illustration of instability of solid cluster structure, where solid structure (fcc, hcp, dh) remains but location and number of structural units changes significantly. The clusters are composed of: (a, b) 450, and (c) 700 atoms represented by coloured balls, as shown in Figure 3. Cluster structures are: (a) decahedral with a characteristic linear chain of dh units and five fcc sectors at 200 000 MC cycle, (b) regular polycrystalline with 3 ic local centres (only one is visible) at 158 000 MC cycle, and (c) defective crystalline in the form of fcc-hcp parallel layers. On the right, plots of the specific heat of the clusters against $T^*$ are shown; arrows and dashed line indicate the position of the clusters and the freezing point (to nondisappearing solid state) on the temperature scale, respectively.

It should be mentioned that the cluster size with $N \approx 400$ as a limit between dynamical- and transient-coexistence region is practically equal to the transition size found by detection of the smallest frozen clusters showing close-packed structure instead of the ideal icosahedral or a regular polyicosahedral one [34] This correlation may be related with structural properties of liquid LJ clusters where small clusters reveal a layered icosahedral-like structure preferring icosahedral atom arrangement [34]. This may also facilitate the fluctuations of cluster state in the coexistence region.

Explanation of different structural states of LJ clusters should be found from analysis of the cluster free energy $F$ with respect to the number of solid-state atoms calculated by using the simulation data. A similar approach was followed recently by Nam et al. [35] while explaining the creation of icosahedral nanoclusters instead of more stable fcc phase when gold clusters are frozen. Very instructive are also arguments given by Berry [31], who analysed theoretically the equilibrium between solid and liquid clusters and predicted the existence of one or two minima in the free energy. Therefore, it is expected that the small LJ clusters are characterised by two local minima, near completely liquid and solid states. The minima are separated by relatively low energy barrier possible to be overcome during a simulation run. When only one minimum for nearly solid or liquid cluster exists or the difference between the minima is too large ($\Delta F \gg k_{\mathrm{B}}T$) observation of one state is expected. This does not exclude, however, some structural changes near the stable state, which would lead to acceptable changes in the free energy around the minimum of $F$. This is the case of the large liquid LJ clusters showing the transient coexistence.

The free energy of solidified clusters near the freezing certainly has the minimum not corresponding to the totally ordered cluster. This may be inferred from the observation of the cluster structure when the cluster is already solidified. Some atoms, mainly near the surface, are not included into the structure or can oscillate between (a) solid unit and disordered one, and (b) different solid structural units. Three examples are given in Figure 4, which shows snapshots of large clusters having the internal structure of (a) decahedron, (b) polyicosahedral type, and (c) layered cluster, i.e. defective crystalline cluster with defects in the form of parallel stacking faults. It may be seen that the cluster from Figure 4a loses and rebuilds an external part of its structure. The average ordering of the shown cluster was estimated to be only 68% of that obtained at

$T^* = 0.05$, when the ordering parameter is defined according to reference [27] as the number of structural units divided by the number of internal atoms. In Figure 4b the initial solid-type structure increases its size and rearranges to a regular polyicosahedral structure with three separated ic units. The other type of structural instability, visible in Figure 4c, has the form of a back-and-forth transition between hcp and fcc units, which was commonly observed in the present study on dense-packed planes near the cluster surface.

Due to the fcc-hcp instability clusters very rarely attain pure crystalline structure in the form of hcp cluster, where two dense-packed surface planes are present. One of the pure hcp clusters is shown in Figure 4c for $N = 700$ and 292 000 MC cycle. The ideal fcc clusters, characterised by 8 surface dense-packed planes, have never been observed. This can be explained by the surface structural instability, which leads to a relatively easy creation of hcp surface layers on one or more of the 8 dense-packed surface planes and strongly disfavours the formation of exclusively fcc units on the cluster surface.

The structural changes in solid clusters are associated with changes in the cluster energy; this is practically equal to the system energy $U$ due to negligible number of vapour atoms. However, the observed energy change in solid clusters is usually much smaller than in the case of freezing or during fluctuations of cluster state in the coexistence region. Therefore, the specific heat from equation (3) can reveal large instability of cluster structure only when the peak connected with phase transition/freezing is absent, i.e. when solidification occurs during the equilibration period (Fig. 4a). When one dominant solidification peak is present, it hides the neighbouring (on temperature scale) smaller peaks, while at a certain distance only some humps appear on the specific heat curve (Fig. 4c). An important exception are large structural changes inside solid phase, which can change significantly the system energy $U$. Figure 4b presents an interesting case, where a radical increase in the size of solid phase accompanied by structure rearrangement to energetically preferred regular polyicosahedral cluster leads to the formation of a large peak in $C_V$.

## 5 Determination of freezing temperature from structural analysis

Cluster freezing is a structural change which can be detected not only by a release of the potential energy but also by creation of new atom ordering. Therefore, in the course of simulations structural units were identified in the cluster every 10th MC cycle at all of the analysed cluster sizes. The cluster ordering is characterised by calculating the averaged number of structural units for every temperature stage. It was found earlier [27] that in liquid 201-atom clusters the fcc, hcp and decahedral structural units practically do not appear, while icosahedral structural units are present usually in 1 to 3 units. A similar situation occurs in the case of the clusters reported here,

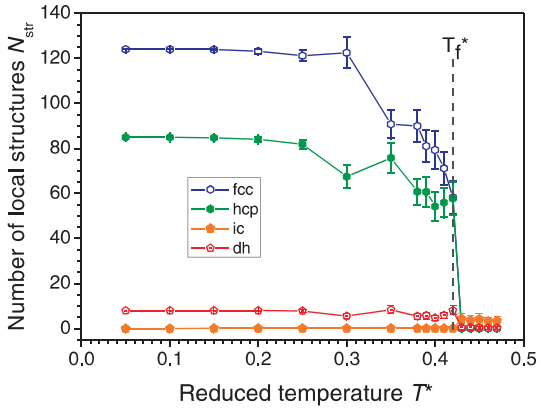


**Fig. 5.** (Colour online) Change in the number of local structural units detected during cooling a 450-atom cluster characterised by curve B in Figure 2a. Vertical bars indicate the value of the standard deviation of $N_{str}$.

although the number of icosahedral units $N_{ic}$ in the liquid clusters fluctuates during simulations and depends on their size $N$. For example, the average value of $N_{ic}$ near the transition point is: 1.1, 2.3, 4.0, 5.0 and 6.8 when the size is $N = 55$, 201, 450, 700 and 923, respectively. For comparison, a maximum number of solid-like units in the liquid cluster is observed for $N = 923$ near the transition point and is equal to 0.2, 0.5 and 0.5 for fcc, hcp and dh units, respectively. The values of $N_{fcc}$, $N_{hcp}$ and $N_{dh}$ are much lower when smaller cluster sizes and higher temperatures are analysed.

A typical temperature dependence of the number of structural units on cluster temperature is illustrated in Figure 5 for the 450-atom cluster, the same one which was characterised by the curve B and C in Figure 2. Two characteristic features may be observed. First, there is an abrupt increase in the average number of fcc, hcp and dh structural units during the cluster solidification. The second feature is a relatively large value of the standard deviation of $N_{fcc}$ and $N_{hcp}$ explained by the instability of solid cluster structure below or at the transition temperature. Therefore, to determine precisely the presence of the solid phase in a cluster the following simple criterion for the number of local structures was used:

$$\langle N_{fcc}\rangle > 1 \text{ or } \langle N_{hcp}\rangle > 1 \text{ or } \langle N_{dh}\rangle > 1, \qquad (5)$$

where the angular brackets denote averaged values in the entire averaging period. The averaging enables to omit detection of transient solid structures in the coexistence region, if they are relatively short-lived.

First attempts of determination of the freezing temperature $T_f^*$ by analysing $N_{str}(T^*)$ with the use of criterion (5) revealed that in small clusters ($N \leq 147$) the solid structure often emerges first and subsequently disappears in the next cooling stage to form once again a solid phase at a lower temperature. It occurs in several, from 4 up to 8, among the 21 analysed clusters. Solid structure in larger clusters is more stable. It does not disappear or only 1 or 2 cases of the structure disappearance are observed for the analysed size $N \geq 201$. The complete instability

of the newly-formed solid phase is a manifestation of the cluster structure transitions between solid-like and liquid-like states in the coexistence region above the freezing point as discussed in Section 4. To overcome this ambiguity, a lower temperature of formation of stable solid phase was always considered. In spite of this care, some small clusters losing their solid-like structure below this lower temperature were still registered. Therefore, criterion (5) is not sufficiently reliable to determine the freezing, but is sufficient for easy detection of the solid-liquid transition temperature $T^*_{\rm tr}$.

The structural changes inside one dominating phase (liquid or solid) and, especially, fluctuations of state between liquid and solid may create a severe obstacle in determining and understanding cluster freezing. Therefore, a serious effort was made to find evolution of cluster structure in the coexistence region and its close neighbourhood. For this purpose, simulation data carrying information about cluster structure statistics saved every 2000th MC cycle were used. While analysing the data it became evident that fluctuations in the total number $N_{\rm s}$ of solid-like units ($N_{\rm s} = N_{\rm fcc}+N_{\rm hcp}+N_{\rm dh}$) are large. In the liquid state $N_{\rm s}$ may oscillate near zero rarely attaining a value higher than 1. However, in the coexistence state the number of solid-like units sometimes can radically increase reaching a value comparable with that encountered during freezing, and then falls down to a liquid-like level as illustrated in Figure 6b. A proportion of simulation time spent by the cluster in solid vs. liquid state increases significantly with decreasing temperature.

The dynamical coexistence was found frequently in small clusters with $N \leq 147$, but was also observed in the case of larger clusters with $N = 201$, 222, and 309. On the other hand, the lower limit for the transient coexistence seems to be $N = 450$, where only one case of birth and dead of a larger solid-type nucleus was observed. However, here the nucleus was recorded to reach only $N_{\rm s} = 5\%N$, which is equivalent to 18% of solid centres formed during a typical freezing at this size. Thus, the fluctuations of state lead to a temporary solidification of most atoms in a cluster of $N \leq 309$, while larger clusters are characterised by their tendency to solidification, engaging only a small part of the internal atoms. The differences in the evolution of small and large clusters are clearly illustrated in Figure 3.

In order to analyse more precisely large structural changes during cooling, the alternative criterion for the detection of solid-like cluster structure was used in the form:

$$N_{\rm s} = N_{\rm fcc} + N_{\rm hcp} + N_{\rm dh} \geq 10\%N. \qquad (6)$$

When most of the records of $N_{\rm s}$ at a given simulation stage (i.e. at a given $T^*$) fulfil the above criterion while the remaining satisfy the relation $N_{\rm s} \geq 2$, the cluster is regarded as solid-like. When none passes criterion (6) and most of them satisfy $N_{\rm s} = 0$ or 1, the cluster is assumed to be liquid-like. When only a part of structural data satisfies this criterion while for others $N_{\rm s} = 0$ or 1, the cluster is treated to be in the coexistence state.

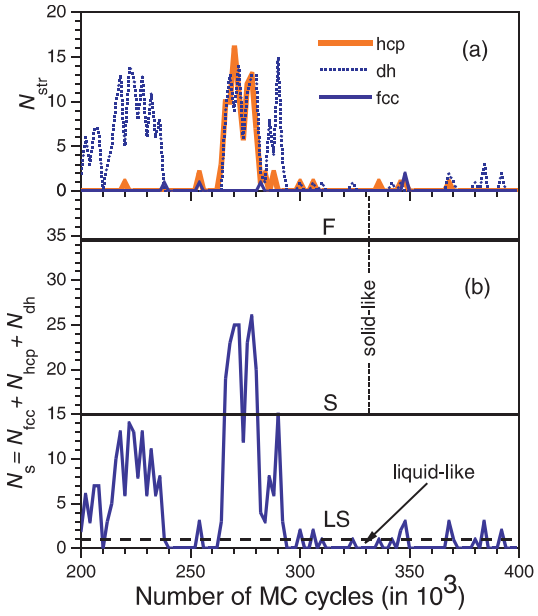


**Fig. 6.** (Colour online) (a) Change in the number of structural units of fcc, hcp and dh type detected every 2000th MC cycle in a cluster composed of 147 atoms at the cooling stage $T^* = 0.36$. (b) Fluctuations in the number of solid-like units $N_{\rm s}$ in the same cluster with respect to limiting lines showing minimum value of $N_{\rm s}$ in: (LS) intermediate liquid-solid cluster, and (S) solid cluster according to condition (6). Regions of liquid and solid cluster states are indicated, while line F represents the averaged value of $N_{\rm s}$ in a frozen cluster of the same size at $T^* = 0.35$.

The last situation is illustrated in Figure 6 for a cluster with $N = 147$ at the temperature $T^* = 0.36$, i.e. just above the freezing. Here one can see that large fluctuations of $N_{\rm hcp}$ and $N_{\rm dh}$ in Figure 6a lead to very large changes of $N_{\rm s}$ in Figure 6b. The plot of $N_{\rm s}$ manages to reach the region of solid-like cluster (above the line S positioned according criterion (6)) in the period 266 000 to 280 000 MC cycles. However, the cluster spends much simulation time below the line LS where it is classified to be in a liquid-state. In Figure 6b there are also positions of $N_{\rm s}$ points observed between LS and S line. This region is called here as the intermediate liquid-solid state. When one analyses $N_{\rm s}$ data to classify the cluster state at a given simulation temperature, special attention must be paid to differentiate between the coexistence state and freezing, when a simulation ends with a period of a radical increase of $N_{\rm s}$ value. If it stabilises at $N_{\rm s}(T^*_{\rm f})$ (line F in Fig. 6b), it denotes the occurrence of stable solidification, i.e. freezing during the averaging period. Criterion (6) in conjunction with the procedure described above is strong enough for proper detection of the freezing point. As was proved by additional manual inspection of cluster structural data, none of the clusters loses the solid-like structure below the freezing temperature determined in this way.

The transition and the freezing temperatures for a given cluster size $N$ and a cluster simulation run were determined independently in two ways, i.e. using criteria (5) and (6). Due to the statistical character of solidification,

**Table 2.** Average value of the cluster transition $T^*_{\rm tr}$ and freezing temperature $T^*_{\rm f}$ calculated by using all 21 values obtained by applying (a) criterion (5), and (b) criterion (6), respectively, for detection of a stable solid phase in the LJ cluster of the mean size $N$.

| Size | (a) | | (b) | |
|---|---|---|---|---|
| $N$ | $\langle T^*_{\rm tr}\rangle$ | $\sigma_{T^*_{\rm tr}}$ | $\langle T^*_{\rm f}\rangle$ | $\sigma_{T^*_{\rm f}}$ |
| 55 | 0.290 | 0.013 | 0.273 | 0.011 |
| 62 | 0.274 | 0.014 | 0.257 | 0.010 |
| 75 | 0.295 | 0.009 | 0.280 | 0.010 |
| 81 | 0.307 | 0.015 | 0.289 | 0.011 |
| 110 | 0.329 | 0.014 | 0.308 | 0.011 |
| 147 | 0.351 | 0.008 | 0.335 | 0.013 |
| 201 | 0.372 | 0.009 | 0.369 | 0.007 |
| 222 | 0.379 | 0.012 | 0.379 | 0.011 |
| 309 | 0.401 | 0.013 | 0.399 | 0.011 |
| 450 | 0.421 | 0.012 | 0.421 | 0.011 |
| 561 | 0.434 | 0.010 | 0.434 | 0.010 |
| 700 | 0.450 | 0.013 | 0.449 | 0.013 |
| 810 | 0.447 | 0.011 | 0.446 | 0.010 |
| 923 | 0.453 | 0.010 | 0.450 | 0.013 |

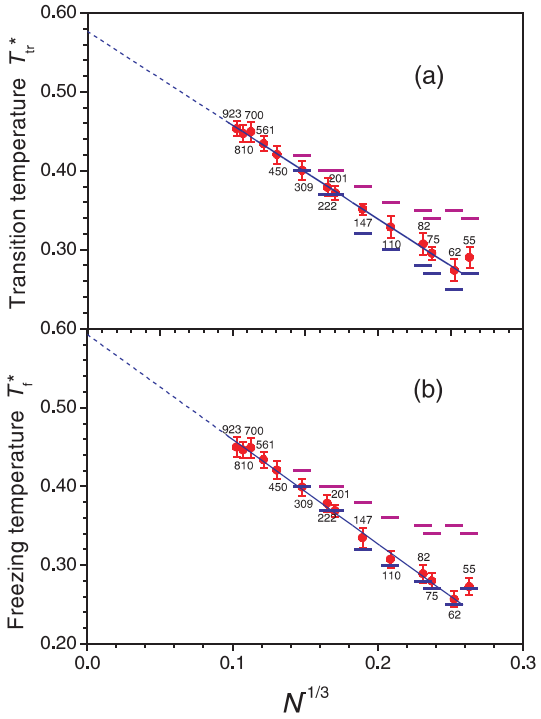


**Fig. 7.** (Colour online) Size dependence of (a) transition and (b) freezing temperature obtained by detection of stable solid-like cluster structure with use of criterion (5) and criterion (6), respectively. Error bars represent standard deviations in $T^*_{\rm tr}$ and $T^*_{\rm f}$. Calculated linear approximation (solid line) in the range from $N = 62$ to 923 is extrapolated (dashed line) to reach the bulk value $T^*_{\rm f}(\infty)$. Horizontal bars denote lower and higher limit (identical in (a) and (b)) of the coexistence region.

not all of the obtained temperatures have the same value for a given $N$. Therefore, for both criteria the obtained 21 values of $T^*_{\rm tr}$ and $T^*_{\rm f}$ for the chosen $N$ were averaged. Since the data are numerous enough, it was possible to obtain the standard deviation $\sigma_{T^*_{\rm tr}}$ and $\sigma_{T^*_{\rm f}}$ directly from its definition. Both data for all cluster sizes and the two applied criteria for freezing detection are collected in Table 2. When these values are presented for each cluster size in Figure 7, it is evident that both the transition and the freezing temperatures of the clusters change exceptionally well linearly with respect to $N^{-1/3}$. For the freezing temperature the dependence can be written in the form:

$$T^*_{\rm f}(N) = T^*_{\rm f}(\infty) - AN^{-1/3}, \qquad (7)$$

where $T^*_{\rm f}(\infty)$ is the interpolated freezing temperature of bulk LJ liquid and $A$ is a proportionality parameter. The $T^*_{\rm tr}(N)$ dependence is also identical to (7), where one replaces 'f' by the subscript 'tr'. Relation (7) is similar to that used by Rytkönen et al. [4] for LJ cluster melting. Linear fitting of the simulation data yields: (a) $T^*_{\rm tr}(\infty) = 0.577$ and $A = 1.19$, and (b) $T^*_{\rm f}(\infty) = 0.593$ and $A = 1.33$ for Figures 7a and 7b, respectively.

The difference in values of the parameters $A$ and $B$ originates from significantly lower values of $T^*_{\rm f}$ obtained, when criterion (6) is applied for smaller clusters (see Tab. 2). It means that a cluster, frozen in the sense of criterion (5), is found more precisely to be in the dynamical or transient coexistence state characterised, respectively, by fluctuations of state or relatively large structural changes inside one state. This is clearly visible in Figure 7a, where the transition temperature of clusters with $N \leq 147$ is located between the limits of the coexistence region for a given $N$. The upper and lower limit was determined by using criterion (6) as maximum and minimum temperature, respectively, at which fluctuations of the cluster state are still observed. Application of the same 10%$N$ criterion corrects significantly the value of the freezing temperature, which is now observable in Figure 7b to be much closer to the limit between the coexistence and the solid-like regions.

The structural criterion (6) is also much more secure for the freezing detection than the analysis of maxima in the specific heat presented in Section 3. When one compares the transition temperature given in column (a) of Table 1 based on energy fluctuation with the freezing temperature given in column (b) in Table 2, lower values of $T^*_{\rm f}$ are usually observed. The exceptions at $N = 450$ and $N = 561$ are attributed to incorrect selection of the peak in $C_{\rm V}(T^*)$.

Careful observation of all distinct maxima in the specific heat curves was done by additional, extensive inspection of cluster structural data saved every 2000th MC trial. In the coexistence region, some global maxima in $C_{\rm V}(T^*)$ result from temporary solidification or melting caused by cluster transition between the two states. Such fluctuations of state precede the cluster freezing. Therefore, the temperature corresponding to the global maximum is very often higher than the freezing temperature, especially at $N \leq 201$. Many smaller peaks are related with fluctuations in the number of the structural units inside liquid or solid cluster, when the existing structure changes but does not disappear.

When the energy differentiation in the form of equation (4) is used to obtain $C_V$, the resulting global maxima agree very well in the cluster size range $450 \leq N \leq 923$ with the freezing temperature from the structural analysis with $10\%N$ criterion. In comparison, systematic temperature divergence of the value $\Delta T^*/2 = 0.005$ is neglected since is caused by the argument of $C_V$ in equation (4). Several small discrepancies observed at each size come from the low sensitivity of equation (4) to detect of an abrupt solidification occurring at the end of simulation stage. At smaller sizes, fluctuations between the states often lead to wrong, overestimated results.

The only considerable deviation from the linearity of $T_f^*(N)$ vs. $N^{-1/3}$ plot in Figure 7b is the smallest cluster with the magic number $N = 55$ corresponding to the closed-shell Mackay cluster. For this size, the separation between extrapolated and observed solidification temperature $T_f^*(55)$ is larger than the calculated standard deviation. This means that solidification of the smallest analysed magic cluster occurs at a temperature significantly higher than that deduced from the approximation line. A similar behaviour was reported by Rytkönen et al. [4] for the melting temperature of $LJ_{55}$ and $LJ_{13}$. In order to observe more details in such deviations, some preliminary simulations and analysis concentrated on small clusters with $N < 55$ were done. However, the proposed method for the freezing temperature determination based on the detection of fcc, hcp and dh units failed. It was unable to determine reasonably the phase transition because fcc and hcp units do not exist in small solid clusters, while the decahedral units are present in a part of the frozen clusters (ca. 50% for $N = 38$). The rest of them is characterised by several interpenetrating icosahedral units.

It should be noted that the value of $T_f^*(\infty) = 0.593$ is lower than the freezing/melting temperature of bulk LJ system equal to $T_m^* = 0.68$ (according to experimental data 84 K for argon [28]). The deviation between $T_m^*$ and $T_f^*(\infty)$ is explained by the fact that $T_f^*(\infty)$ reflects the maximum undercooling attainable in bulk liquid rare gases. In this context, the extrapolated undercooling of 13% calculated from $T_f^*(\infty)$ and $T_m^*$ is in good agreement with the experimental data of about 20% [36] observed under typical conditions. For comparison, simulated nucleation in the bulk LJ liquid occurs during MD simulations at very large undercooling of ca. 40% [36], when the nucleation barrier connected with the critical cluster formation is sufficiently low to be overcome during a reasonable simulation time.

## 6 Summary and conclusions

The new method based on detection of solid-like units in the form of fcc, hcp or decahedral local atom arrangement was applied for the precise determination of the cluster state transitions. The general idea is to apply the cluster structural analysis in association with a criterion determining threshold for solid-like cluster classification. The method based on criterion (6) proved to be the most precise in determining the fluctuations of cluster state during simulations, the coexistence region width and the freezing temperature, which is in contrast to difficulties met using maxima in the specific heat curves. Moreover, the presented results demonstrate that the analysis of specific heat curves obtained from energy fluctuations as well as from energy difference overestimates the cluster freezing temperature due to sensitivity to structural liquid-solid transitions in the coexistence region. Therefore, this temperature is called the transition temperature.

The linear relationship of the size-dependence of cluster freezing temperature, with characteristic proportionality to $N^{-1/3}$, observed for 14 different sizes is in agreement with the formula known from theoretical predictions for cluster melting. The obtained parameters of the approximating straight line precisely determine the border-line between the coexistence state and solid cluster phase for criterion (6) assuming minimum 10% of cluster atoms creates centres of solid-like local structure. The extrapolated freezing temperature $T_f(\infty)$ of the bulk LJ was obtained to be 13% lower than the experimental value, but is close to obtained experimental undercooling.

The smallest cluster with $N = 55$ is an exception from linearity, where the separation between extrapolated and observed solidification temperature is significantly larger than the calculated standard deviation. Analysis of the freezing temperature of smaller cluster revealed that the method based on structural analysis fails. This is due to the absence of fcc and hcp units in all of the frozen clusters with $N < 55$ and the lack of decahedral units in a significant number of them.

The observation of subtle effects associated with the formation and disappearance of a solid phase in the LJ clusters is an important result explained as a manifestation of the dynamical and transient coexistence between liquid-like and solid-like cluster structures. It occurs frequently in small cluster with $N \leq 147$, but was also observed in larger clusters till $N = 309$ when criterion (6) in the form of 10% of cluster atoms as local centres of a solid-like structure applies. Structural changes of smaller amplitudes were also observed in larger liquid clusters beginning from $N = 450$. This does not lead, however, to the formation of the solid phase in the sense of condition (6). The structure instability hinders detection of cluster freezing, when the lifetime expressed in MC cycles of such transient solid structures is comparable with the averaging time at this simulation stage. To overcome this problem, an increase of the number of MC cycles is suggested at simulation stages near the freezing point in the coexistence region, though it results in longer computation time.

The instability of solid phase also occurs after cluster freezing. The solid structure remains as a whole but some atoms lose their specific arrangement in the first shell, which transforms to a disordered shell. This occurs mainly near the surface and may concern a relatively large fraction of atoms with completed first shell, e.g. 32% for the analysed 450-atom cluster. Apart from the solid-to-disordered-state transition, a solid state enlargement and rearrangement as well as permanent back-and-forth

transformations of hcp to fcc planes on the cluster surface, mainly on the dense-packed planes, were observed.

The author thanks Prof. K. Sangwal and Dr K. Wójcik for their advice and constant support. This work was partly financed by the State Committee for Scientific Research (Poland) (KBN) under the grant No. 2 P03B 027 25.

## References

1. P. Pawlow, Z. Phys. Chem. **65**, 1 (1909)
2. C.L. Briant, J.J. Burton, J. Chem. Phys. **63**, 2045 (1975)
3. F. Celestini, R.J.-M. Pellenq, P. Bordarier, B. Rousseau, Z. Phys. D **37**, 49 (1996)
4. A. Rytkönen, S. Valkealahti, M. Manninen, J. Chem. Phys. **108**, 5826 (1998)
5. J. Gspann, Z. Phys. D: At. Mol. Clust. **3**, 143 (1986)
6. L.S. Bartell, J. Huang, J. Phys. Chem. **98**, 7455 (1994)
7. M. Schmidt, R. Kusche, B. von Issendorff, H. Haberland, Nature **393**, 238 (1998)
8. T.P. Martin, U. Näher, H. Schaber, U. Zimmermann, J. Chem. Phys. **100**, 2322 (1994)
9. B.W. van de Waal, *The fcc/hcp Dilemma* (B.W. van de Waal, Twente, 1997)
10. T. Ikeshoji, G. Torchet, M.-F. de Feraudy, K. Koga, Phys. Rev. E **63**, 031101 (2001)
11. F. Baletto, R. Ferrando, Rev. Mod. Phys. **77**, 371 (2005)
12. J. Farges, M.-F. de Feraudy, B. Raoult, G. Torchet, J. Chem. Phys. **84**, 3491 (1986)
13. E.T. Verkhovtseva, I.A. Gospodarev, A.V. Grishaev, S.I. Kovalenko, D.D. Solnyshkin, E.S. Syrkin, S.B. Feodos'ev, Low Temp. Phys. **29**, 386 (2003)
14. P. Shah, S. Roy, C. Chakravarty, J. Chem. Phys. **118**, 10671 (2003)
15. R.S. Berry, J. Jellinek, G. Natanson, Phys. Rev. A **30**, 919 (1984)
16. L.J. Lewis, P. Jensen, J.-L. Barrat, Phys. Rev. B **56**, 2248 (1997)
17. S. Valkealahti, M. Manninen, J. Phys.: Cond. Matter **9**, 4041 (1997)
18. S.C. Hendy, B.D. Hall, Phys. Rev. B **64**, 085425 (2001)
19. H.-S. Nam, N.M. Hwang, B.D. Yu, J.-K. Yoon, Phys. Rev. Lett. **89**, 275502 (2002)
20. F. Baletto, C. Mottet, R. Ferrando, Chem. Phys. Lett. **354**, 82 (2002)
21. X.L. Zhu, X.Z. You, R.G. Xiong, Z.H. Zhou, Chem. Phys. **269**, 243 (2001)
22. J. Huang, L.S. Bartell, J. Phys. Chem. **106**, 2404 (2002)
23. K.E. Kinney, S. Xu, L.S. Bartell, J. Phys. Chem. **100**, 6935 (1996)
24. J.D. Honeycutt, H.C. Andersen, J. Phys. Chem. **91**, 4950 (1987)
25. N. Quirke, Mol. Simul. **1**, 249 (1988)
26. Z.H. Jin, H.W. Sheng, K. Lu, Phys. Rev. B **60**, 141 (1999)
27. W. Polak, A. Patrykiejew, Phys. Rev. B **67**, 115402 (2003)
28. C. Kittel, *Introduction to Solid State Physics*, 5th edn. (Wiley, New York, 1976), Chap. 3
29. S. Sugano, *Microcluster Physics* (Springer Verlag, Berlin Heidelberg, 1991)
30. R.S. Berry, Melting and Freezing of Clusters: How They Happen and What They Mean, in: *Clusters of Atoms and Molecules I*, edited by H. Haberland (Springer, Berlin, 1995), Chap. 2.8
31. R.S. Berry, Microscale Therm. Eng. **1**, 1 (1997)
32. H. Matsuoka, T. Hirokawa, M. Matsui, M. Doyama, Phys. Rev. Lett. **69**, 297 (1992)
33. D. Schebarchov, S.C. Hendy, J. Chem. Phys. **123**, 104701 (2005)
34. W. Polak, *Evidence for size-transition in internal structure of frozen Lennard-Jones clusters*, in preparation
35. H.-S. Nam, N.M. Hwang, B.D. Yu, D.-Y. Kim, J.-K Yoon, Phys. Rev. B **71**, 233401 (2005)
36. P.R. ten Wolde, M.J. Ruiz-Montero, D. Frenkel, J. Chem. Phys. **104**, 9932 (1996)